

Accepted Manuscript

Open-field PET: Simultaneous brain functional imaging and behavioural response measurements in freely moving small animals

Andre Z. Kyme, Georgios I. Angelis, John Eisenhuth, Roger R. Fulton, Victor Zhou, Genevra Hart, Kata Popovic, Mahmood Akhtar, Will J. Ryder, Kelly Clemens, Bernard Balleine, Arvind Parmar, Giancarlo Pascali, Gary Perkins, Steven R. Meikle

PII: S1053-8119(18)32132-3

DOI: <https://doi.org/10.1016/j.neuroimage.2018.11.051>

Reference: YNIMG 15456

To appear in: *NeuroImage*

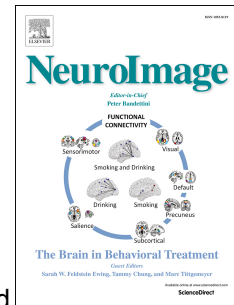
Received Date: 24 May 2018

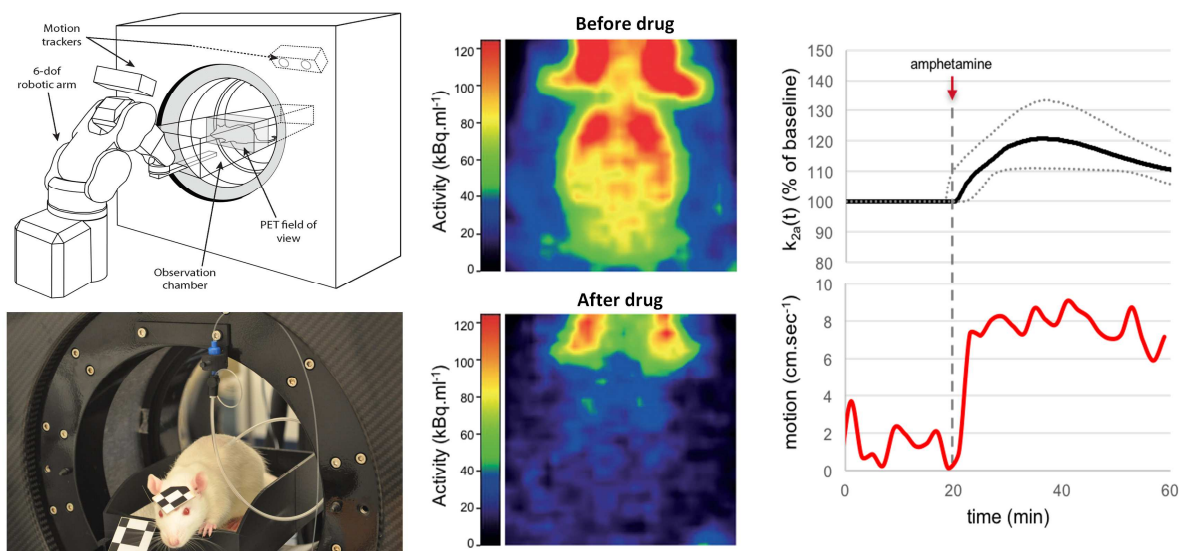
Revised Date: 1 November 2018

Accepted Date: 27 November 2018

Please cite this article as: Kyme, A.Z., Angelis, G.I., Eisenhuth, J., Fulton, R.R., Zhou, V., Hart, G., Popovic, K., Akhtar, M., Ryder, W.J., Clemens, K., Balleine, B., Parmar, A., Pascali, G., Perkins, G., Meikle, S.R., Open-field PET: Simultaneous brain functional imaging and behavioural response measurements in freely moving small animals, *NeuroImage* (2018), doi: <https://doi.org/10.1016/j.neuroimage.2018.11.051>.

This is a PDF file of an unedited manuscript that has been accepted for publication. As a service to our customers we are providing this early version of the manuscript. The manuscript will undergo copyediting, typesetting, and review of the resulting proof before it is published in its final form. Please note that during the production process errors may be discovered which could affect the content, and all legal disclaimers that apply to the journal pertain.





Open-field PET: Simultaneous brain functional imaging and behavioural response measurements in freely moving small animals

Andre Z. Kyme^{a,b,c,*†}, Georgios I. Angelis^{b,c†}, John Eisenhuth^c, Roger R. Fulton^{b,c,d}, Victor Zhou^{b,1}, Genevra Hart^{e,2}, Kata Popovic^{b,c}, Mahmood Akhtar^{b,c,3}, Will J. Ryder^{b,c,4}, Kelly Clemens^f, Bernard Balleine^{e,2}, Arvind Parmar^{b,g}, Giancarlo Pascali^{b,g}, Gary Perkins^g, Steven R. Meikle^{b,c}

Affiliations

- a. Biomedical Engineering, School of AMME, Faculty of Engineering and IT, The University of Sydney, Sydney, NSW 2006, Australia
- b. Imaging Physics Laboratory, Brain and Mind Centre, The University of Sydney, Sydney, NSW 2006, Australia
- c. Faculty of Health Sciences, The University of Sydney, Sydney, NSW 2006, Australia
- d. Department of Medical Physics, Westmead Hospital, Sydney, NSW 2145, Australia
- e. Brain and Mind Centre, The University of Sydney, Sydney, NSW 2006, Australia
- f. School of Psychology, University of New South Wales, Sydney, NSW 2052, Australia
- g. Australian Nuclear Science and Technology Organisation, Sydney, NSW 2234, Australia

† Joint first authors

* Correspondence: Andre Z. Kyme, Ph.D.

Biomedical Engineering, School of AMME, Faculty of Engineering & IT
The University of Sydney

Darlington, NSW 2006, Australia

E: andre.kyme@sydney.edu.au

T: +61 2 9351 2260

M: +61 406268121

1. Now with Central Queensland University, Mackay, QLD 4740, Australia
2. Now with the Decision Neuroscience Laboratory, School of Psychology, University of New South Wales, Sydney, NSW 2052, Australia
3. Now with Faculty of Engineering, University of New South Wales, Sydney, NSW 2052, Australia

4. Now with Concord Hospital, Sydney, NSW 2137, Australia

ACCEPTED MANUSCRIPT

Abstract

2 A comprehensive understanding of how the brain responds to a changing environment requires
3 techniques capable of recording functional outputs at the whole-brain level in response to external
4 stimuli. Positron emission tomography (PET) is an exquisitely sensitive technique for imaging brain
5 function but the need for anaesthesia to avoid motion artefacts precludes concurrent behavioural
6 response studies. Here, we report a technique that combines motion-compensated PET with a
7 robotically-controlled animal enclosure to enable simultaneous brain imaging and behavioural
8 recordings in unrestrained small animals. The technique was used to measure in vivo displacement
9 of [¹¹C]raclopride from dopamine D2 receptors (D2R) concurrently with changes in the behaviour
10 of awake, freely moving rats following administration of unlabelled raclopride or amphetamine.
11 The timing and magnitude of [¹¹C]raclopride displacement from D2R were reliably estimated and,
12 in the case of amphetamine, these changes coincided with a marked increase in stereotyped
13 behaviours and hyper-locomotion. The technique, therefore, allows simultaneous measurement of
14 changes in brain function and behavioural responses to external stimuli in conscious unrestrained
15 animals, giving rise to important applications in behavioural neuroscience.

16

17 **Keywords:** Awake animal PET, behaviour, kinetic modelling, motion correction, dopamine D2
18 receptors, drug challenge

19 **1. Introduction**

20 Interactions between an animal and its environment are complex. How these interactions are
21 encoded in the brain and used to guide future behaviour is an area of intense study, exploiting a
22 wide range of microscopic and macroscopic measurement techniques such as patch clamp
23 recordings and 2-photon imaging (Chen et al. 2013). For the most part, these techniques are
24 performed with the animal under anaesthesia and/or rigidly fixed in a stereotactic frame. More
25 recently, several of these methods have been extended to enable localised recordings in awake,
26 freely moving animals following surgical implantation or attachment of the requisite probe (Belle et
27 al. 2013, Helmchen et al. 2001, Vyazovskiy et al. 2011). However, these methods are invasive,
28 prone to imprecise sampling of the neuronal population of interest and confined to small pre-
29 determined anatomical regions of the brain. A more complete understanding of how the brain
30 responds to a changing environment requires new techniques capable of recording functional
31 outputs at the whole-brain level in response to external stimuli, while retaining cell and receptor
32 type specificity.

33 High resolution small animal positron emission tomography (PET) has the potential to advance our
34 understanding of the signalling pathways involved in cognition and behaviour under normal and
35 pathological conditions. With the appropriate choice of positron-emitting radiopharmaceutical, this
36 method provides a quantitative 3D map of blood flow, metabolism or receptor-ligand binding
37 throughout the rodent brain, including animal models of disease (Chatziioannou 2002), with pico-
38 molar sensitivity. Importantly, since PET is a non-invasive, non-terminal procedure, it also enables
39 the longitudinal study of these processes during normal development and disease progression,
40 including responses to therapeutic intervention or environmental stressors. Conventional PET
41 technology requires the animal to remain motionless throughout the 1- to 2-hour scanning
42 procedure, typically achieved by anaesthesia and rigid fixation of the head. However, the routine
43 use of anaesthesia not only perturbs many of the neurological parameters of interest, such as blood
44 flow, neural-hemodynamic coupling and receptor binding (Nakao et al. 2001, Tantawy et al. 2011),
45 it also precludes the use of functional imaging to relate changes in neurotransmitter activity and
46 receptor binding to behavioural adaptation in response to environmental cues or drug administration
47 (Cherry 2011).

48 Several approaches have been developed in an attempt to mitigate the confounding effects of
49 anaesthesia, although limitations with all of these methods have restricted their utility. For example,
50 one approach is to inject the PET tracer, then to present the desired stimulus while the animal is
51 conscious, and later to anaesthetise the animal for imaging (Thanos 2013). This approach is mainly
52 limited to PET tracers that are irreversibly trapped in the cell, such as 2-deoxy-2-[¹⁸F]fluoro-D-

53 glucose (FDG), thus allowing a delayed ‘snapshot’ image of brain function that reflects the peri-
54 stimulus state. While similar methods have been used in conjunction with reversible receptor-
55 binding PET ligands (Patel et al. 2008, Tantawy et al. 2011), they do not enable real-time
56 measurement of transient changes in receptor binding at the onset of the stimulus. Another approach
57 is to rigidly attach a miniature PET detector ring to the head of the animal (Vaska et al. 2004, Shulz
58 et al. 2011). Although this method enables dynamic imaging of awake rats with receptor-binding
59 PET ligands, together with a limited range of behavioural assays, it requires invasive surgery to
60 attach the imaging apparatus to the head and the inertia of the attached detector ring restricts natural
61 movement of the animal. Finally, the feasibility of tethering the skull of a mouse to a rigid head
62 fixation device while undergoing PET imaging in the conscious state has been demonstrated
63 (Mizuma et al. 2010). However, this technique requires extensive training and acclimatisation,
64 provides for only a limited variety of behavioural response assays, and is subject to the confound of
65 stress-induced physiological changes.

66 To overcome these limitations, we developed an open-field PET imaging technique that enables the
67 brain of an unrestrained rat to be imaged in an unmodified small animal PET scanner, while
68 simultaneously recording behavioural outputs following the delivery of controlled stimuli. The
69 technique combines advanced motion estimation and motion-compensated image reconstruction
70 methods, a robotically-controlled animal enclosure conducive to behavioural testing, and a
71 tracer/drug delivery protocol that accommodates a freely moving animal. Here we describe the
72 open-field PET system and associated methodology and demonstrate the simultaneous
73 measurement of changes in regional D2 receptor (D2R) binding and behavioural responses to
74 pharmacological stimuli in conscious, unrestrained rats.

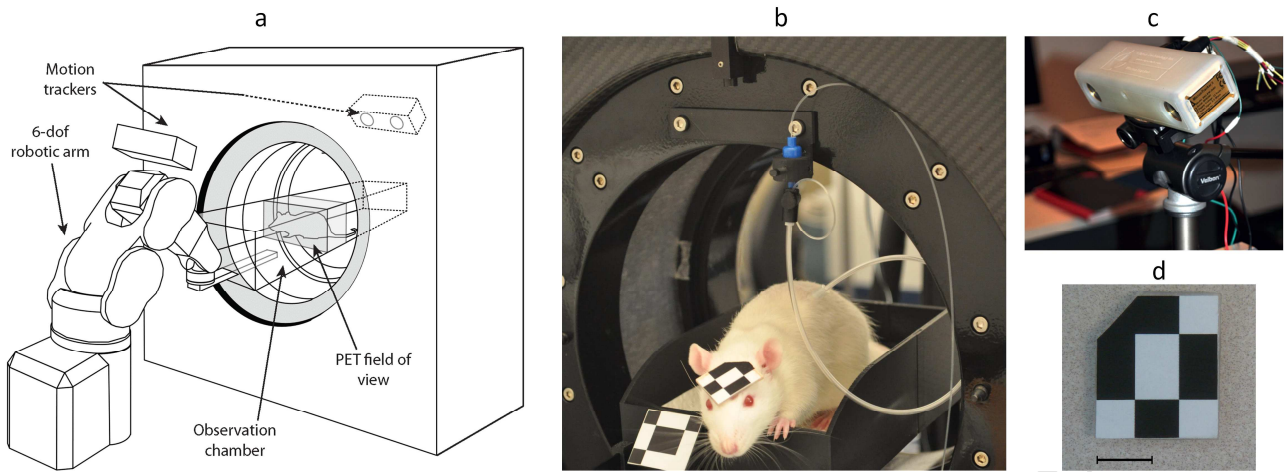
75

76 **2. Methods**

77 **2.1 Open-Field PET System Overview**

78 The open-field PET system comprises a commercial PET scanner, optical motion tracking and a
79 custom designed motion adaptive animal enclosure attached to a 6-axis robotic arm (fig. 1a).
80 Motion tracking (fig. 1b) from both ends of the PET gantry enables measurement of the changing
81 position and orientation of a small lightweight marker attached to the forehead of the animal (fig.
82 1c, d). Reconstruction of quantitatively accurate, motion-corrected PET images requires accurate
83 calibration and synchronisation of head pose estimates with data acquired by the PET scanner
84 (Kyme et al. 2008, Kyme et al. 2012) and an event-by-event (list mode) motion-corrected image
85 reconstruction algorithm (Rahmim et al. 2008).

86



87

88 **Figure 1: Open-field PET experimental setup**

89 (a) The experimental setup for the open-field PET technique, consisting of an unmodified small
 90 animal PET system, a robot-controlled animal enclosure and optical motion tracking devices at the
 91 front and rear of the PET gantry; (b) the catheterised, freely moving animal connected to a syringe
 92 pump (not visible in this figure) via a swivelled injection line; (c) the motion tracking system which
 93 uses a pair of CCD cameras to determine the rigid-body motion of three printed markers, one small
 94 lightweight marker attached to the animal's forehead (b and d, scale bar = 1 cm), another marker
 95 attached to the enclosure, and a third marker attached to the PET scanner (not visible in this figure).
 96

97 **2.1.1 PET scanner.** The open-field PET system is built around the microPET Focus 220 preclinical
 98 PET scanner (Preclinical Solutions, Siemens Healthcare Molecular Imaging, Knoxville, TN, USA),
 99 which comprises lutetium oxyorthosilicate (LSO) scintillation detectors coupled to photomultiplier
 100 tubes. The Focus has a bore diameter of 220 mm, a transaxial FoV of 190 mm and an axial FoV of
 101 76 mm. Spatial resolution and coincidence photon detection sensitivity at the centre of the FoV are
 102 1.3 mm FWHM and 3.4%, respectively (Tai et al. 2005). All data were recorded in list mode
 103 (event-by-event) format and stored locally for offline processing.

104

105 **2.1.2 Motion tracking.** Two MicronTracker Sx60 binocular tracking systems (ClaroNav, Toronto,
 106 Canada) were located at opposite ends of the scanner bore (fig. 1a) to track the rigid-body pose
 107 (position and orientation) of the animal's head and the enclosure with 0.2 mm (RMS) positional
 108 accuracy. Both trackers were oriented at 45 degrees declination and positioned 0.5 m from the
 109 centre of the scanner FoV in accordance with the optimised geometry described in Kyme et al.
 110 (2012). The two trackers were spatially calibrated to a common reference frame in which all marker
 111 measurements were reported, regardless of which tracker actually detected the marker. The tracking
 112 frame was also cross-calibrated to the PET frame so that PET lines of response could be corrected
 113 for motion offline.

114 Three separate markers were tracked during our experiments: a marker attached to the animal's
 115 head (fig. 1c, d), a marker attached to the moving enclosure (fig. 1c), and a reference marker

116 permanently fixed to the PET gantry. The reference marker enabled convenient updating of the
117 tracker-scanner cross-calibration in each new experiment without having to repeat the cross-
118 calibration procedure. Details of this approach are described in Kyme et al. (2011). The enclosure
119 marker comprised two large L-shaped facets, one at each end of the enclosure. Position
120 measurements of the enclosure were fed to the robot controller software (section 2.1.4) in real time
121 to prevent collisions between the enclosure and gantry as the position of the enclosure was adjusted
122 in response to animal motion. The head marker comprised a single L-shaped facet on a 3D-printed
123 substrate (fig. 1d), which was affixed to a small shaved patch on the animal's forehead (fig. 1c)
124 using a drop of cyanoacrylate (super glue). Using this approach, markers remained firmly attached
125 to the scalp for several hours.

126 During an experiment, the changing pose of each marker was measured at 30 Hz. The position (i.e.
127 just the (x, y, z) component) of the head marker was transformed to the PET coordinate frame in
128 real time and input to the robot controller software for adaptive enclosure position control in
129 response to animal motion. The full pose (i.e. position and orientation component) of the head
130 marker was stored for offline motion compensation of the PET data. Triggering of the front- and
131 rear-side trackers occurred simultaneously using a square-wave generator (TTL, positive polarity,
132 half-duty cycle, 24-30 Hz). Each trigger pulse initiated sensor exposure for each tracker and also
133 triggered a square pulse (TTL, positive polarity, 15 ms duration) from the front-side tracker to the
134 gating input on the PET scanner. Receipt of this pulse at the scanner gating input resulted in the
135 insertion of a gating 'tag-word' in the PET event data stream. Matching of these tag-words with the
136 triggered pose measurements allowed us to synchronise the two data streams for motion
137 compensation. To enable rapid (5 ms) exposure of the CCD cameras in the tracking systems, we
138 bounced the light from two 1000-watt halogen work lights off the ceiling to give a diffuse
139 illuminance of approximately 450 Lux inside the scanner FoV. The lights were positioned
140 symmetrically on either side of the scanner, out of direct sight of the animals.

141
142 **2.1.3 Animal enclosure.** The motion-adaptive animal enclosure is a structurally rigid, lightweight
143 and minimally attenuating box consisting of multiple 3D-printed interlocking sections of
144 acrylonitrile butadiene styrene (ABS) thermoplastic supported by carbon fibre ribs which run the
145 length of the enclosure and thread the sections together for additional stability and to resist flexing
146 about the longitudinal axis. The enclosure is 120 mm wide and adjustable in length from 200-500
147 mm. All of our experiments were performed using a length of 220 mm. The enclosure is designed
148 with an optional computer-interfaced lever press and reward delivery mechanism. This allows it to
149 be used during a PET study either as a simple observation chamber for studying animal behaviour,

150 or as an operant chamber for instrumental conditioning experiments. A 3D-printed adaptor was
151 used to secure the carbon fibre ribs and to mount the enclosure to the robot end-effector.

152

153 **2.1.4 Robot positioning and control.** The 6-axis robot (Epson C3-A601S, Seiko Corp., Japan)
154 used to adaptively position the animal enclosure in response to animal motion was mounted to a
155 custom-built trolley adjacent to the PET gantry. The robot was programmed to translate the
156 enclosure in response to measured head movements. These translations were sufficiently slow and
157 smooth to avoid startling the animal. The basic motion control algorithm for compensatory
158 enclosure positioning is described in detail in Zhou et al. (2013). However, rather than perform
159 compensatory movements of the enclosure using the sector-based method described previously, we
160 adapted the algorithm to translate the enclosure along the exact straight-line trajectory from its
161 current position to the centre of the scanner field-of-view (FoV). In addition, whenever the head
162 marker was obstructed from both trackers (i.e. no updated head position information was available),
163 the robot would automatically return the marker to the centre of the scanner FoV based on its last
164 known position. This 'recovery mode' was intended to rapidly restore tracking and, thereby,
165 maintain close to uninterrupted robotic compensatory motion.

166

167 **2.1.5 Motion compensation and image reconstruction.** All reconstructions were performed using
168 10 iterations and 10 subsets of an iterative ordered subsets expectation maximisation (OSEM) list
169 mode reconstruction algorithm incorporating motion compensation according to the method
170 described in Rahmim et al. (2008). The acquired list-mode events were pre-corrected for motion on
171 an event-by-event basis using the pose information obtained from the motion tracker (Zhou et al.
172 2008). Corrections for normalisation were included within a motion-dependent, time-weighted
173 sensitivity image (Rahmim et al. 2008), while events were corrected for photon attenuation using a
174 transmission-less calculated attenuation correction approach (Angelis et al. 2013, Angelis et al.
175 2014). Scatter correction was not performed since the scatter fraction is <15% for the rat brain. We
176 also applied a shift-invariant resolution model during the reconstruction based on an empirically
177 defined resolution kernel corresponding to the scanner resolution at the centre of the FoV.

178

179 **2.2 Animal Management**

180 **2.2.1 Animals.** Male wild-type Sprague-Dawley rats were used for the imaging experiments. The
181 animals were healthy, pathogen-free, drug naïve and had not been used in previous experimental
182 procedures. For the reproducibility study (section 3.1), four 10-week old animals (mean weight
183 304 ± 26 g, range 256-330 g) were scanned on two consecutive days. For the simultaneous open-
184 field PET and behavioural response study (section 3.2), three 15-week old animals (mean weight

185 442±17.6 g, range 421-465 g) were scanned on two consecutive days. Animals were group-housed
186 in ventilated cages and maintained on a 12-h:12-h light:dark cycle with food and water *ad libitum*.
187 All animal management and experimentation was performed in accordance with protocols approved
188 by the University of Sydney Animal Ethics Committee and consistent with National Institutes of
189 Health guidelines.

190

191 **2.2.2 Surgery.** One week after arrival rats were implanted with a chronic indwelling catheter in the
192 right jugular vein. Rats were anaesthetised with 2-3% inhalation isoflurane in oxygen (2 L/min)
193 and injected with a pre-emptive analgesic (Carprofen, 5 mg/kg s.c.). A custom-made catheter
194 consisting of silastic tubing (internal diameter (ID) 0.5 mm, outer diameter (OD) 1.5 mm, Dow
195 Corning) was inserted 25 mm into the jugular vein, terminating in the heart. The distal end passed
196 subcutaneously to exit posterior to the scapulae and terminated with a 22-gauge back mount
197 cannula (Plastics One, VA, US). The back mount was secured in place with a suture and flushed
198 daily with cephazolin sodium antibiotic (0.2 mL, 100 mg/mL) in sterile saline (0.9%). Following
199 three days of recovery, heparin (150 I.U/mL) was added to the antibiotic solution to minimise
200 catheter blockage. Catheters were flushed daily with heparinised cephazolin for the remainder of
201 the first week and then every 2-3 days thereafter. Rats were allowed seven days to recover from
202 surgery before commencing acclimatisation, training and imaging experiments.

203

204 **2.2.3 Acclimatisation protocol.** One week after surgery the rats were systematically acclimatised
205 to the imaging environment and open-field apparatus over four days: day 1 was basic
206 familiarisation with the scanner environment for 30 minutes without a head marker or tethered
207 catheter; on days 2-4 the animals were habituated for 45 minutes to the full experimental
208 conditions, including the attached head marker, tethered catheter and robotic motion compensation.
209 The lighting (room lights and auxiliary lights) and positions of all stationary apparatus (video
210 cameras, syringe pump, computers, motion tracking systems and cabling) required for imaging on
211 days 5 and 6 were identical during the acclimatisation sessions to avoid introducing novel visual
212 cues. Video data were recorded for each animal to observe behavioural patterns during
213 acclimatisation. Posture, gait, respiration and activity for all animals were found to be normal.

214

215 **2.3 Radiotracer and drug infusion**

216 [¹¹C]Raclopride was synthesised according to Perkins et al. (2014). A 30 cm cannula connector
217 made of flexible plastic tubing (ID 1.93 mm, OD 2.74 mm, Plastics One) was used to connect the
218 jugular port on the scapulae to a stainless steel swivel (Instech Laboratories Inc.) fixed to the
219 scanner gantry. Cannula tubing (ID 0.58 mm, OD 0.96 mm, Microtube Extrusions) was inserted

220 through the connector for tracer and drug infusion. The thick connector tubing provided protection
 221 against the animal chewing through the infusion line. From the swivel, the cannula tubing
 222 connected to a syringe loaded in a syringe pump (Harvard Pico Plus). Altogether, the length of
 223 cannula tubing from syringe to animal was chosen to give 320 μL dead volume. This enabled us to
 224 safely load 250 μL of tracer in the infusion line prior to beginning a slow bolus infusion at the start
 225 of the imaging study. The tracer was infused over 38 s by pumping 600 μL of sterile saline (0.9%)
 226 through the line at 400 $\mu\text{L}\cdot\text{min}^{-1}$. This volume also completely flushed the line once the tracer
 227 volume was expelled. For drug infusion, 140 μL was loaded into the line and infused over 15 s by
 228 pumping 400 μL of sterile saline through the line at 400 $\mu\text{L}\cdot\text{min}^{-1}$. The total injected volume for
 229 each rat was 1.35 mL ($\sim 5\%$ total blood volume). Raclopride was administered as unlabelled
 230 raclopride in 0.9% sterile saline (100 μL , 2 $\text{mg}\cdot\text{kg}^{-1}$). Amphetamine was administered as D-
 231 amphetamine dissolved in 0.9% sterile saline (100 μL , 2 $\text{mg}\cdot\text{kg}^{-1}$).
 232

233

2.4 Data Analysis

234 **2.4.1 PET data analysis.** Transient changes in physiology following drug administration has been
 235 shown to cause time-dependent fluctuations in radiotracer delivery and clearance (Alpert et al.
 236 2003), thus conventional steady state models are invalid. Accordingly, decay-corrected PET time-
 237 activity curves were fitted with the linear parametric neurotransmitter PET (lp-ntPET) model
 238 (Normandin et al. 2012), which is a generalisation of the multi-linear reference tissue model
 239 (MRTM) (Ichise et al. 2003) that includes a time-varying term to describe non-steady state
 240 condition. The lp-ntPET model leads to the following operational equation that describes the tracer
 241 concentration in the target region-of-interest (ROI) (the striatum in our case), C_T , as a function of
 242 time, t :

$$C_T(t) = R_1 C_R(t) + k_2 \int_0^t C_R(u) du - \int_0^t (k_{2a} + \gamma h_i(u)) C_T(u) du \quad (1)$$

243 where C_R is the tracer concentration in the reference ROI (cerebellum) and $\theta = [R_1, k_2, k_{2a}, \gamma]$ are the
 244 model coefficients. The transient perturbation of the system is modelled by $h_i(t)$ which represents
 245 the time course of the activation, with γ encoding the magnitude of the effect. As in Normandin et
 246 al. (2012), we modelled $h_i(t)$ as a series of gamma variate functions spanning a wide range of
 247 feasible shapes and possible times of onset (from 10 to 40 minutes at 1.5 min intervals). The lp-
 248 ntPET model was fitted to the PET data using a weighted least squares and basis pursuit strategy.

249 The key model output from this fitting procedure in ligand displacement studies is the time-
 250 dependent tracer efflux from the compartment representing specifically bound tracer:
 251

$$k_{2a}(t) = k_{2a} + \gamma h(t)$$

252

253 where $h(t)$ represents the gamma variate function that best fits the data and describes the activation
 254 effect. Fitting the lp-ntPET model as described provides model parameter point estimates but does
 255 not tell us about the reliability of those estimates. To evaluate the reliability we used the Monte
 256 Carlo based Approximate Bayesian Computation (ABC) algorithm (Marin et al. 2012). This method
 257 involves conducting a very large number (~millions) of trials using model parameters drawn
 258 randomly from a prior distribution, in our case an uninformative uniform prior. For each trial, the
 259 model-based PET curve is estimated according to equation (1) and compared with the measured
 260 PET curve. The trial is either accepted or rejected based on the sum of squared differences between
 261 the two curves and a predetermined threshold. After many such trials, the model curves which are
 262 accepted have sufficient statistics to form a histogram of parameter estimates that provide an
 263 excellent approximation of the posterior probability density functions (PDF) of those parameters.
 264 As well as computing PDFs, we also calculated median and 95% confidence intervals for the $k_{2a}(t)$
 265 term from the sub-population of accepted model curves, i.e. the successful trials.

266

267 **2.4.2 Motion data analysis.** Locomotor activity response as a function of time was determined
 268 directly from the motion tracking data and reported in units of $\text{cm}\cdot\text{s}^{-1}$.

269

270 **2.4.3 Behavioural data analysis.** In addition to the locomotor response, stereotyped and non-
 271 stereotyped behaviours exhibited by the rat during the open-field PET scans were analysed
 272 manually using a time sampling procedure adapted from Kelley (1998). The rat was observed every
 273 minute throughout each of the open-field PET scans and scored according to the presence or
 274 absence of each of nine behaviours, which are summarised in Table 1. A behavioural score was
 275 calculated as the proportion of time the rat engaged in each behaviour.

276

277 **Table 1: Categorisation of animal behaviours**

Behaviour	Description
Sleep	Asleep or immobile in resting position for greater than 30 seconds
Groom	Head or body grooming
Locomotion	Repetitive (>3 reps) gross movement of whole body or head and shoulders, e.g. rearing towards the top of the scanner then leaning towards the bottom
Head-up sniff	Head tilted upwards, sniffing in reared or non-reared position
Head-down sniff	Head tilted downwards, sniffing the bottom of the scanner or chamber

Mouth movements	Non-specific oral movements, tongue protrusions, air licking
Chew	Chewing the chamber flooring, walls etc.
Perch	Positioned with hind legs on or near the wall of the chamber, body balanced over the edge, front paws either in the air or on the wall of the chamber
Head bob	Fast upward and downward head movements

278

279 **3. Experiments**280 **3.1 Reproducibility of the open-field technique**

281 We evaluated the ability of the open-field technique to reliably estimate changes in D2R binding in
 282 the brains of freely moving rats. Four adult male Sprague-Dawley rats were scanned on two
 283 consecutive days. For both scans the rats were administered [¹¹C]raclopride (mean 48±18 MBq,
 284 0.84±0.16 nmol) via the indwelling jugular vein catheter and imaged in the open-field PET system
 285 for 60 minutes. For one PET scan, the animals were administered 2 mg.kg⁻¹ of unlabelled raclopride
 286 20 minutes after tracer injection. Based on previous studies, this dose of raclopride is expected to
 287 occupy close to 100% of available D2 receptors in the rat brain and cause nearly complete
 288 displacement of the tracer from D2R binding sites (Hume et al. 1995, Hume et al. 1998). For the
 289 other PET scan, an identical protocol was used except that a saline vehicle was administered at 20
 290 min instead of unlabelled raclopride. The order of the scans was counterbalanced across animals.
 291 From the reconstructed and decay-corrected dynamic frames we generated curves representing the
 292 regional temporal characterisation of the increased efflux rate (displacement) from the striatum.

293

294 **3.2 Simultaneous open-field PET and behavioural response studies**

295 The purpose of the previous experiment was to demonstrate that the open-field PET method can
 296 reliably estimate changes in dopamine receptor occupancy. To illustrate the use of the approach in
 297 combined behavioural and receptor-ligand imaging studies, we measured D2R displacement in the
 298 cold raclopride challenge and following administration of the psychostimulant drug, amphetamine.
 299 In addition to a nearly complete displacement of the radiotracer from the D2 receptors, injection of
 300 a pharmacological dose of cold raclopride may also lead to reduced locomotor activity and
 301 avoidance behaviours (Hillegaart and Ahlenius 1987). On the other hand, amphetamine stimulates
 302 endogenous dopamine release from synaptic vesicles causing indirect competition with
 303 [¹¹C]raclopride for post synaptic D2R binding sites. This intervention is also expected to result in
 304 robust behavioural changes, such as hyperactivity and stereotypy (Schiorring et al. 1979). For the
 305 amphetamine challenge, three adult male Sprague-Dawley rats underwent two open-field PET
 306 studies on consecutive days. For each scan, the animal was injected with [¹¹C]raclopride (mean
 307 39±15 MBq, 0.82±0.35 nmol) via the indwelling jugular vein catheter and imaged in the open-field

PET system for 60 minutes. For the first PET scan, the animal was administered 540 μ l of a saline vehicle via the catheter 20 minutes after tracer injection. For the second PET scan, the same protocol was used except that 2 mg.kg⁻¹ of amphetamine was administered together with the saline vehicle. Dynamic PET data were analysed by least squares fitting of striatal time-activity curves with the lp-ntPET model which estimates the magnitude and timing of tracer displacement from the receptor-ligand complex (Normandin et al. 2012). To assess the reliability of model estimates, the posterior probability density distributions of displacement parameters were further analysed using ABC (Marin et al. 2012). The velocity of the animal's head in the horizontal plane was calculated at 2-min intervals throughout the PET study. These data were used as a proxy for locomotor activity and compared with the timing and magnitude of [¹¹C]raclopride displacement. In addition, video acquired throughout each PET study was analysed using a time sampling procedure adapted from Kelley (1998) to measure a variety of stereotypical and non-stereotypical behaviours.

During all open-field imaging experiments the rats were free to move around the enclosure and, since it had no roof, were also able to lean over the sides. The floor of the enclosure was covered in absorbent towels to collect excrement and radioactive urine safely. All experiments were filmed from the front of the scanner using a video camera positioned 0.7 m from the centre of the scanner FoV.

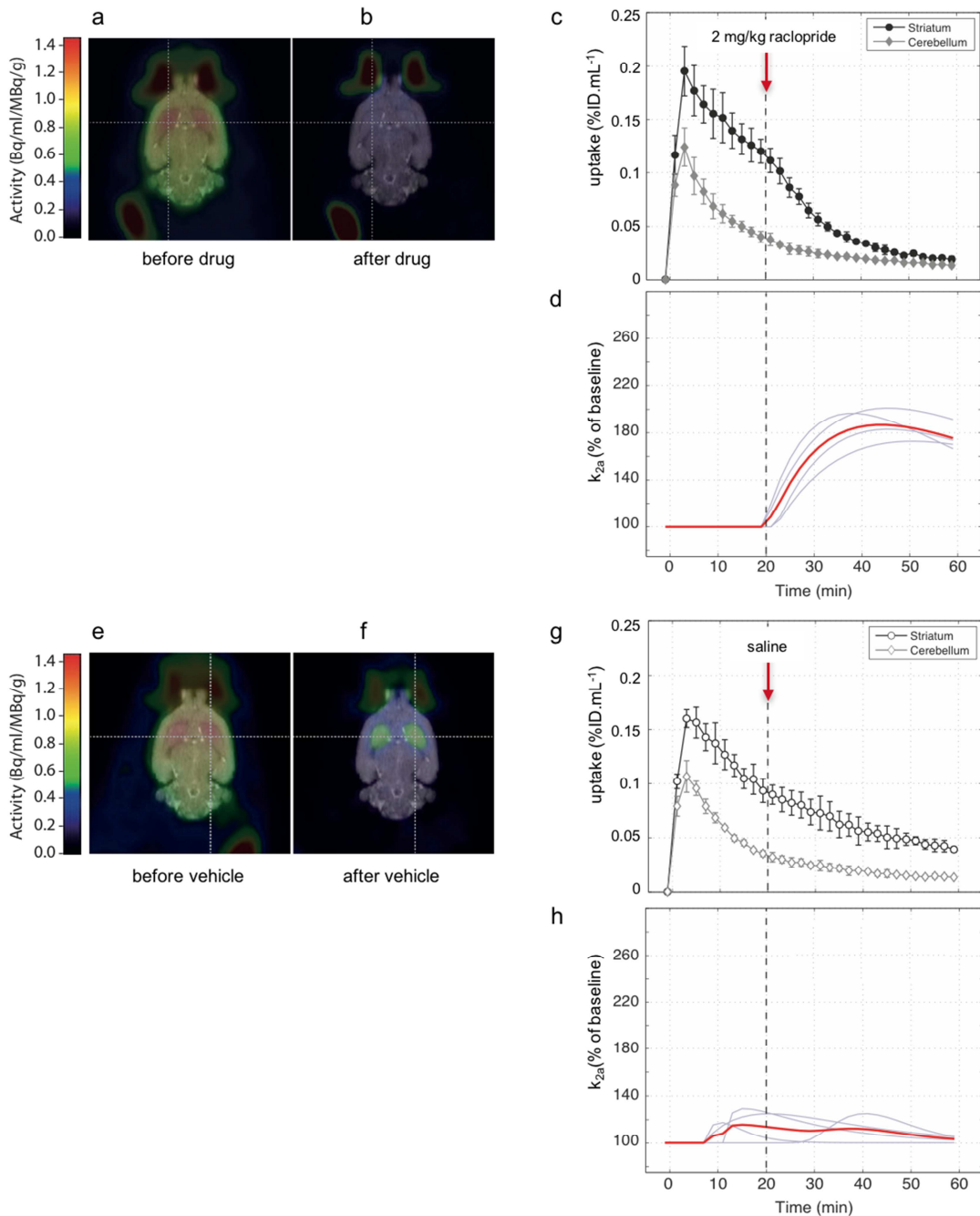
4. Results

4.1 Reproducibility of the open-field PET technique

Motion-corrected images integrated over the 20 minutes immediately prior to drug/saline injection and for the last 20 minutes of the scan are shown for the drug and saline vehicle scans of one representative rat in figures 2a,b and 2e,f, respectively. Decay-corrected striatal and cerebellar tracer uptake curves averaged across all four animals, after normalising for injected dose and body weight, are shown in figures 2c and 2g for the drug and vehicle scans, respectively.

The dynamic data were analysed by least squares fitting of individual striatal time-activity curves with the lp-ntPET ligand displacement model using the corresponding cerebellar curve as the input function (see Section 2.4.1). The model-estimated ligand displacement curves $k_{2a}(t)$ for the drug challenge and vehicle-only scans are shown in figures 2d and 2h, respectively. The time-activity curves and displacement curves demonstrate a high degree of inter-subject reproducibility. Estimated time of onset of the displacement caused by injection of unlabelled raclopride, averaged across the four animals, was $t_d = 19.5 \pm 1.2$ min, which agrees well with the time of drug administration, and the peak amplitude of displacement was 1.85 ± 0.2 x baseline. The small magnitude, temporally misaligned false positive displacements seen in the null condition (fig. 2h)

342 are typical features of the lp-ntPET method when applied to noisy PET data (Normandin et al.
 343 2012).
 344



345

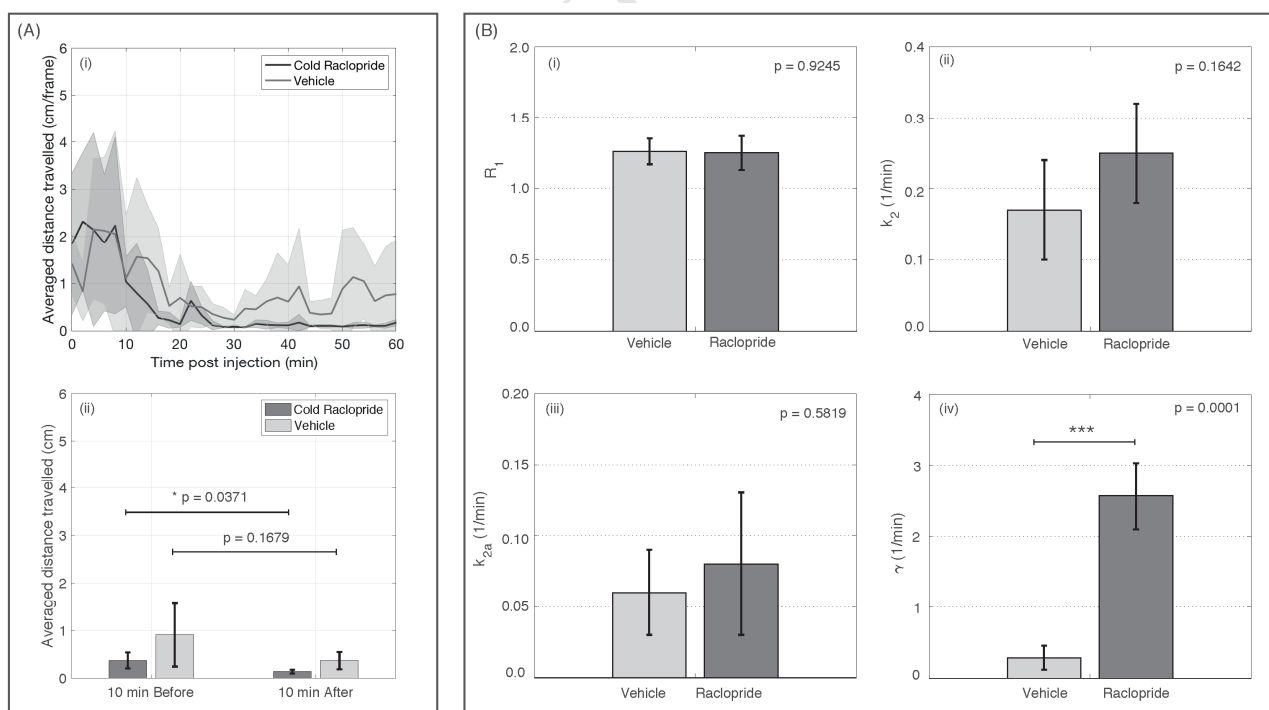
346 **Figure 2: Reproducibility of the open-field PET technique**

347 (a) Motion-corrected PET data showing the integrated [¹¹C]raclopride distribution in the brain of a
 348 representative freely moving rat over the first 20 minutes of the study (prior to the administration of
 349 unlabelled raclopride), superimposed on a spatially registered MRI brain template; (b) reconstructed
 350 PET image integrated over the last 20 minutes of the study, after administration of unlabelled
 351 raclopride; (c) PET time-activity curves averaged across four animals (mean \pm 1 s.d) for striatal and
 352 cerebellar regions of interest; and (d) the four individual (grey) and mean (red) estimated D2R
 353 displacement (k_{2a}) curves obtained from kinetic modelling of the dynamic PET data in (c). The
 354 images and graphs in panels e-h are the corresponding data obtained from the animals administered
 355 a saline vehicle 20 minutes into the PET study instead of unlabelled raclopride.

356
357
358
359
360
361
362
363
364
365
366
367
368
369
370
371
372
373
374
375
376

4.2 Simultaneous open-field PET and behavioural response

4.2.1 Cold raclopride. Figure 3A.i shows locomotor activity averaged across the 4 subjects (the shaded areas correspond to the ± 1 standard deviation envelope) binned into 2-min frames (i.e. equal to the duration of the functional frames) for both the saline-vehicle and cold raclopride injections. To quantitatively assess the change in behaviour before and after injection of the drug or vehicle, we averaged the distance travelled by the animals 10 minutes before injection and 10 minutes after (fig. 3A.ii). There was a slight reduction in locomotor activity after injection of cold raclopride which reached statistical significance ($p < 0.05$), whereas saline had no significant effect on behaviour ($p = 0.1679$). We believe that the behavioural effect of raclopride did not reach a greater level of significance due to the ‘floor effect’, where the animals were already exhibiting relatively low levels of motor activity prior to injection. Figure 3B shows the group-average parameter estimates of the 1p-ntPET model, highlighting a significant change in the non-steady state parameter γ describing the magnitude of activation (i.e. increased efflux rate) after drug administration, and insignificant differences for the steady-state parameters, R_1 , k_2 and k_{2a} .



377
378
379
380
381

Figure 3: Motion and kinetic model parameters for the cold raclopride challenge.

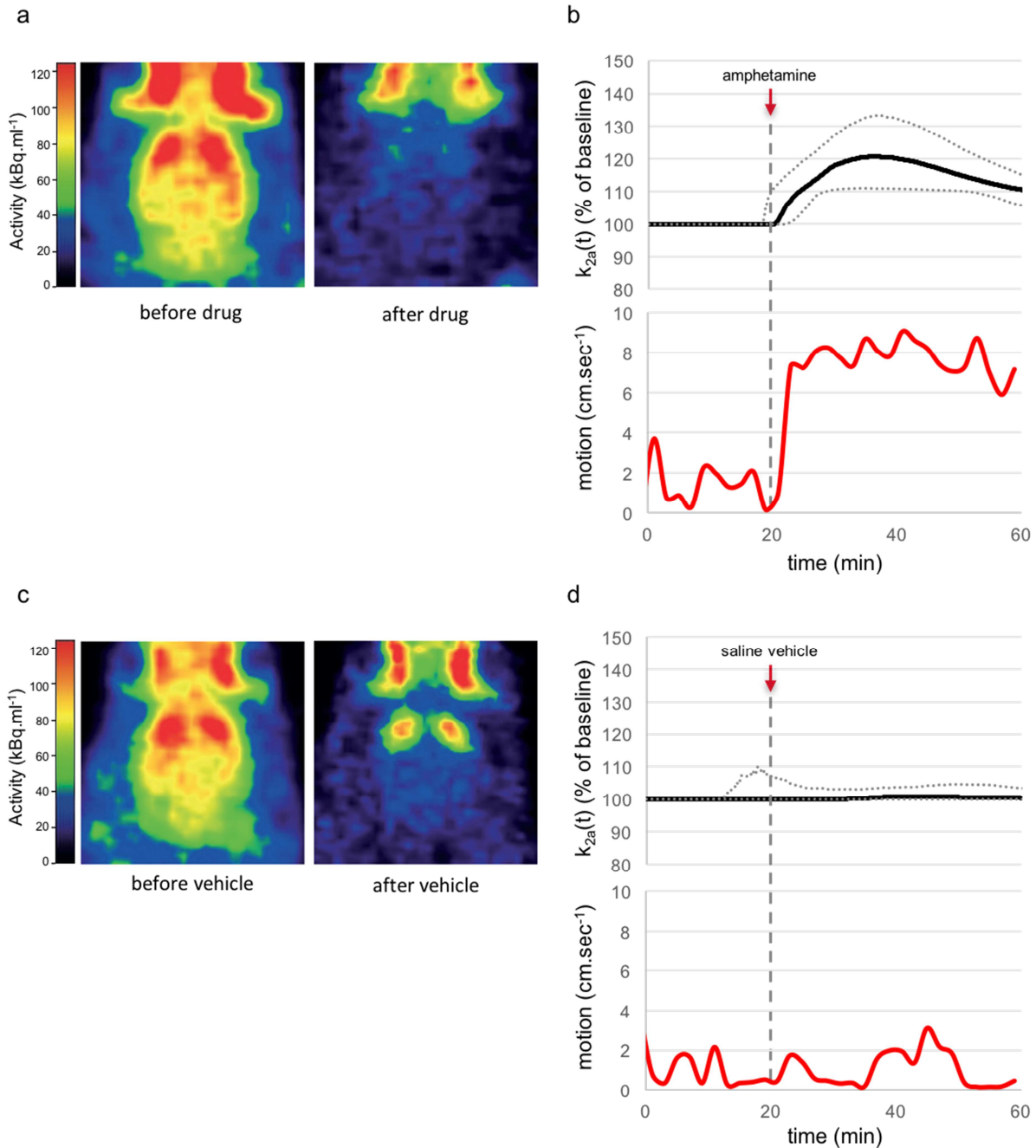
(A.i) Average distance travelled as a function of time (shaded areas correspond to ± 1 standard deviation) for the cold raclopride/saline scans; (A.ii) average distance travelled over 10 minutes before and 10 minutes after the injection of cold raclopride/saline; (B) estimated kinetic model

382 parameters averaged across 4 animals for the cold raclopride/saline injection experiments (asterisks
383 indicate significance at the $p < 0.001$ level; paired t -test).
384

385 **4.2.2 Amphetamine.** Figure 4a shows the motion-corrected [^{11}C]raclopride distribution in the brain
386 integrated over the first 20 minutes of the study (left panel), i.e. prior to amphetamine
387 administration, and over the last 20 minutes of the study (right panel), i.e. after amphetamine
388 administration, for a representative subject. An appreciable displacement of the specific D2R
389 binding signal in the striatum is seen in the post drug administration image. The lp-ntPET model
390 output curve (fig. 4b, upper panel) also indicates a clear displacement of the tracer from D2R
391 binding sites whose time of onset is consistent with the time of drug administration and reaches a
392 peak amplitude of 120% of baseline 15-20 minutes after drug administration. The displacement also
393 correlated with a pronounced increase in head motion (average post-drug motion = 543% of
394 average pre-drug motion) that was sustained until the end of the imaging study (fig. 4b, lower
395 panel). There was no change in specific D2R binding in the striatum observed on either the
396 integrated PET images (fig. 4c) or displacement curves (fig. 4d, upper panel) in the saline vehicle
397 scan. The differences between the pre- and post-vehicle images, including extra-striatal regions, can
398 be explained by changes in blood flow (which are accounted for by the lp-ntPET model) and
399 normal biological clearance. Similarly, there was no observable change in behaviour following
400 vehicle administration (fig. 4d, lower panel).

401 Figure 5A.i shows the averaged locomotor activity across the 3 animals. In contrast to the cold
402 raclopride study, amphetamine produced a clear and sustained increase in locomotor activity shortly
403 after injection of the drug, which is consistent across the 3 animals. Similar to the cold raclopride
404 analysis, we averaged the distance travelled by the animals 10 minutes before and 10 minutes after
405 the injection of the drug (fig. 5A.ii). The injection of amphetamine led to a behavioural effect that
406 was highly significant ($p < 0.001$; paired t -test), whereas saline caused no significant effect
407 ($p = 0.4125$). The change in behaviour due to the injection of amphetamine was also clearly evident
408 by visually observing the animal (fig. 6). We also averaged the estimated kinetic model parameters
409 across the 3 animals (fig. 5B) which shows a highly significant ($p < 0.005$; paired t -test) increase in
410 activation magnitude, γ , for amphetamine compared with vehicle only scans, and small but
411 insignificant decreases in k_2 and k_{2a} . An association between regional DA signalling dynamics and
412 the behavioural effect of the drug is, therefore, clearly evident.

413



414

415

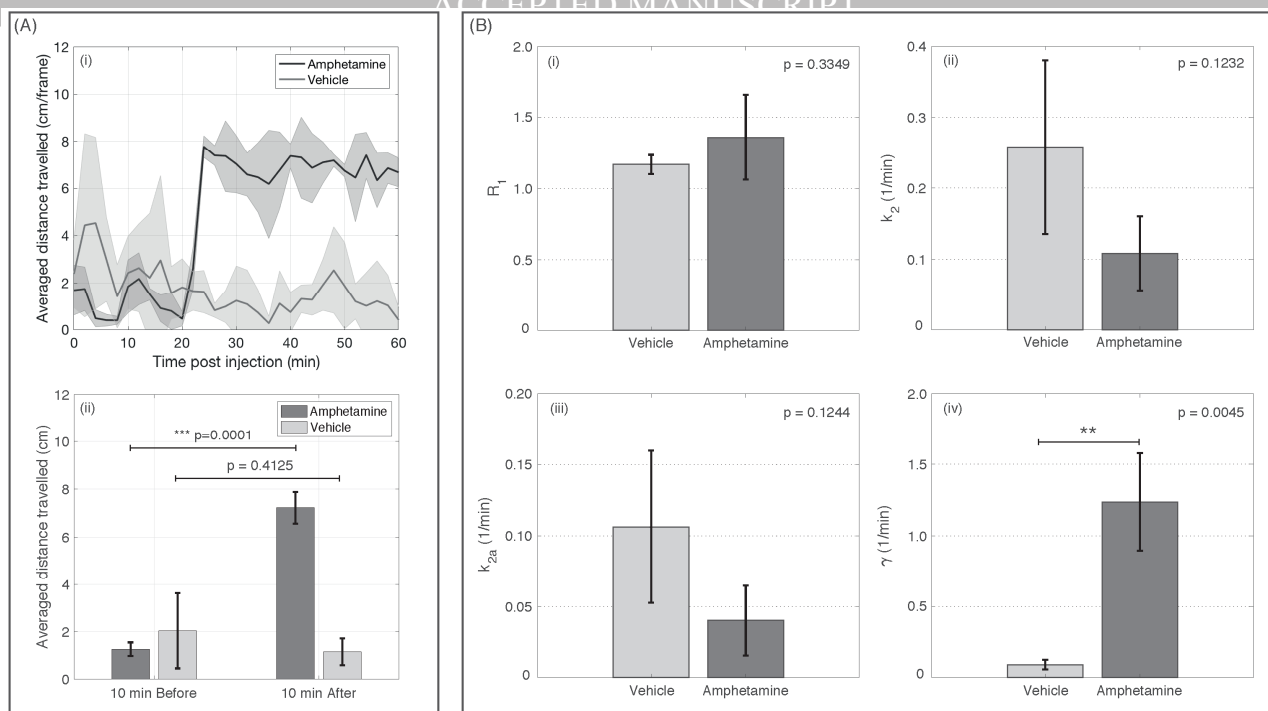
416 **Figure 4: Simultaneous open-field PET and behavioural response to amphetamine challenge**

417 (a) Motion-corrected PET images (co-registered to a MRI brain template) showing the integrated
 418 [¹¹C]raclopride distribution in the brain of a representative freely moving rat integrated over the 20
 419 minutes prior to drug administration (left) and over the last 20 minutes of the study (right); (b)
 420 estimated D2R displacement (k_{2a}) curves ($\pm 95\%$ CI) for the striatum (upper) and the locomotor
 421 activity throughout the PET study (lower) for the animal receiving amphetamine. Panels c and d
 422 show the corresponding tracer distributions, D2R displacement curve and motion data when the
 423 same animal underwent a separate PET scan and received only the saline vehicle 20 minutes after
 424 [¹¹C]raclopride injection.

425

426

427



428

429

430

431

432

433

434

435

436

437

438

439

440

441

442

443

444

445

446

447

448

449

450

451

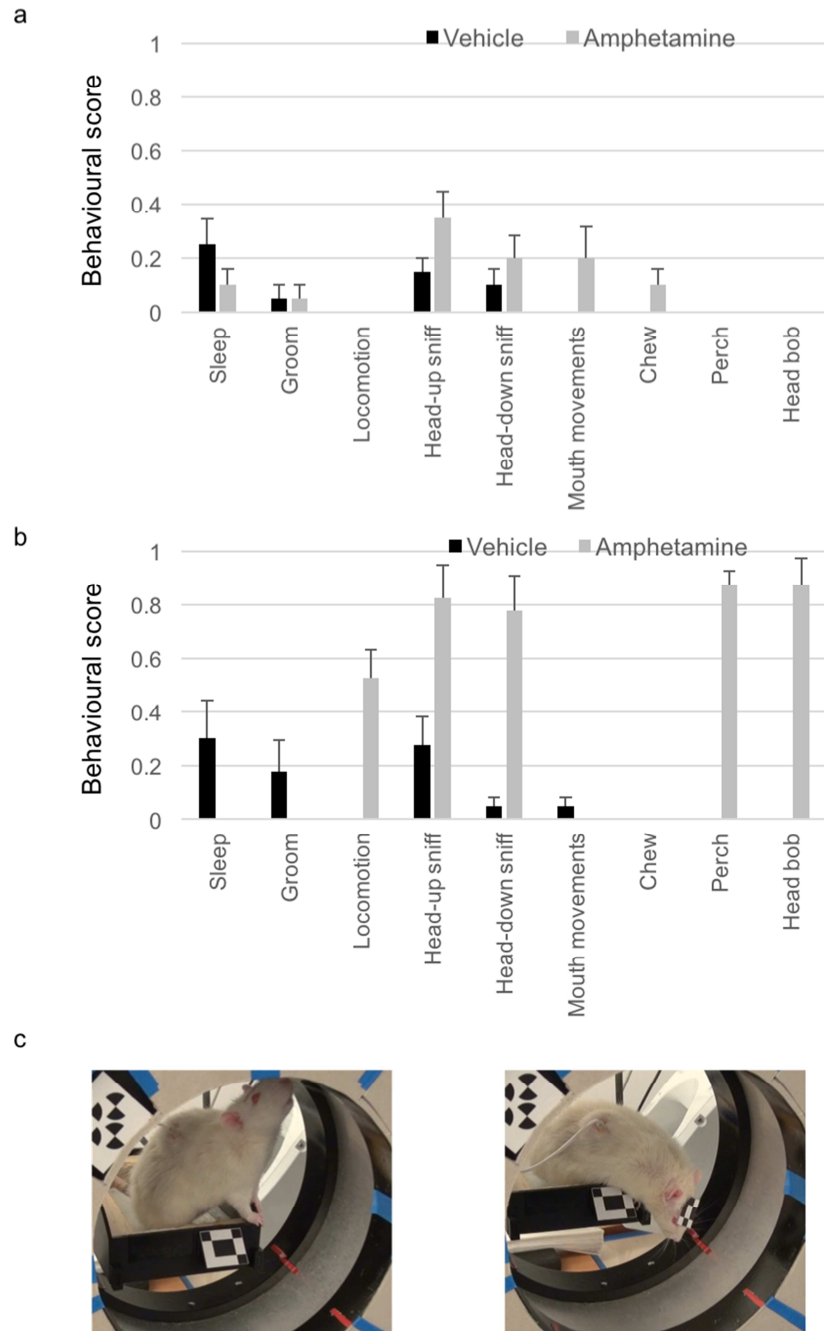
Figure 5: Motion and kinetic model parameters for the amphetamine challenge.

(A.i) Average distance travelled as a function of time (shaded areas correspond to ± 1 standard deviation) for the amphetamine/saline scans; (A.ii) average distance travelled over 10 minutes before and 10 minutes after the injection of amphetamine/saline (asterisks indicate significance at the $p < 0.001$ level; paired t -test); (B) estimated kinetic model parameters averaged across 3 animals for the amphetamine/saline injection experiments (asterisks indicate significance at the $p < 0.01$ level; paired t -test).

Figure 6a shows the behavioural analysis of a representative animal throughout the amphetamine and saline vehicle PET scans. The animal exhibited similar behavioural profiles during the first 20 minutes of each scan, prior to drug or vehicle administration (fig. 6a). Following amphetamine administration (fig. 6b), the rat showed a marked increase in repetitive locomotive stereotyped behaviour. It repeatedly adopted a unique “perched” position and alternately sniffed the base and top of the scanner (fig. 6c). In contrast, following vehicle administration the rat maintained moderate to low levels of sniffing behaviour in a non-perched position and other non-stereotypical behaviours, such as sleeping and grooming. The observed changes in behaviour following amphetamine administration are consistent with previous studies (Lindquist et al. 1977, Schiorring 1979) and can be attributed to activation of the thalamo-striatal pathway via sudden release of endogenous dopamine. Together with the results shown in the previous section and figures 4 and 5, the current study provides evidence of *in vivo* changes in D2R occupancy and simultaneous changes in behaviour due to amphetamine administration to awake, freely moving rats.

450

451



452

453

454 **Figure 6: Analysis of behaviours during open-field PET studies**

455 Analysis of stereotypical and non-stereotypical behaviours exhibited throughout the open-field PET
 456 scans in figures 4 and 5 by a representative rat: (a) behavioural score for a range of different
 457 behaviours (Table 1) during the 20 minutes prior to drug or saline vehicle administration; (b)
 458 behavioural score for a range of different behaviours during the 40 minutes following drug or saline
 459 vehicle administration. Scores are based on the proportion of time spent exhibiting a given
 460 behaviour during each 1 min interval (Kelly 2008), averaged over the full observation period. Error
 461 bars represent standard error of the mean; (c) still frames of the video taken during the open-field
 462 PET study demonstrating stereotypical head-up (left) and head-down (right) sniffing in a perched
 463 position.

464

465

466

467 **5. Discussion**

468 We have developed an open-field PET system that addresses three fundamental limitations of small
469 animal neuroimaging studies: (i) it overcomes the confounding effects of common anaesthetic drugs
470 on neurophysiological parameters such as cerebral blood flow, neurotransmitter release and
471 receptor occupancy (Martin et al. 2006, Ohba et al. 2009); (ii) it enables the study of neurochemical
472 responses to sensory stimuli that require the conscious attention of the animal (Tsukuda et al. 2002);
473 and (iii) it enables the concurrent study of regional neurotransmitter-receptor function and
474 behavioural responses to drugs and other environmental stimuli in conscious, unrestrained animals.
475 All of these advantages can be exploited in longitudinal study designs because the technique allows
476 repeat experiments on the same animal.

477 Using this technique, we demonstrated that it is possible to reproducibly detect and quantify, in
478 awake and freely moving animals, a pharmacologically induced displacement of [¹¹C]raclopride
479 from D2 receptors by administering unlabelled raclopride, with reliable estimates of the magnitude
480 and time of displacement onset. We also demonstrated the concurrent measurement of changes in
481 receptor-ligand binding and behaviour; specifically, we measured changes in D2 receptor binding,
482 locomotion and stereotypy associated with stimulation of dopamine release following the
483 administration of amphetamine to awake, freely moving rats. Importantly, the technology we have
484 developed allows us to reproducibly associate a measurable functional response in the brain to a
485 diverse range of locomotor activity responses – from reduced (e.g. cold raclopride) to extreme
486 increase (e.g. amphetamine) in locomotor activity.

487 Since we are considering a non-steady state regime in which the injection of the drug affects the
488 physiology and the kinetic parameters (especially k_{2a}) in a time dependent manner, conventional
489 models such as the SRTM or MRTM are no longer valid (Alpert et al. 2003). We demonstrated
490 quantifiable displacement in the time-varying receptor binding using the lp-ntPET model
491 (Normandin et al. 2012) in conjunction with statistical confidence modelling using the ABC method
492 (Marin et al. 2012). We believe this is the first study to report the relative magnitude of ligand
493 displacement following drug challenge for awake rodents.

494 To our knowledge, this is also the first report of a complete motion compensation-based solution for
495 freely moving rats during PET imaging. A related approach for single photon emission computed
496 tomography (SPECT) of awake mice was reported by Baba et al. (2013), however the system was
497 limited to tube-bound animals. Several alternative approaches for tracking animal head motion have
498 been reported which could be substituted for our tracking method, providing potential advantages.
499 For example, marker-free tracking based on native features (Kyme et al. 2014) or structured light

500 (Miranda et al. 2017) avoids the problem of head-marker decoupling, and tracking of radioactive
501 fiducials glued to the head avoids the need for additional tracking hardware (Miranda et al. 2018) –
502 though the latter approach is only useful when the animal is inside the FoV. A further motion
503 tracking improvement relates to lighting. Currently, the animals are pre-acclimatised to the visible
504 lighting needed for motion tracking. Although this lighting is diffuse and outside the animal's direct
505 line-of-sight, and we have not observed any evidence that they are perturbed by it, the ability to
506 perform infra-red based tracking (Baba et al. 2013) in ambient or darkened conditions is preferable
507 for nocturnal subjects and would likely facilitate a greater range of experiments.

508 The system described in this report is based on a commercially available small animal PET system
509 without modification, other than replacement of the animal support pallet with a robotically
510 controlled enclosure and a mechanism to synchronise motion tracking and PET data. Thus, the
511 open-field PET system could, in principle, be deployed where there is a suitable commercial small
512 animal PET scanner. However, it has some limitations that may affect performance of the PET
513 study. For example, the robot is programmed to translate the animal enclosure relatively slowly
514 (max speed 1.6 cm.s^{-1}) with smooth acceleration and deceleration to avoid startling the animal. For
515 a typical scan, this may lead to the animal spending on average $< 5\%$ of the time outside the active
516 FoV during a scan, which has a negligible effect on the acquired dynamic data. However, when the
517 animal is more active, such as with an amphetamine challenge, on average it may spend a larger
518 portion of the PET study (approximately 40%) with its brain outside the active FoV of the scanner,
519 resulting in significant loss of counts. Similarly, the animal may move to blind spots (where
520 tracking line-of-sight is obstructed), causing temporary loss of data. While we can account for
521 temporary loss of data within the reconstruction software, it negatively impacts signal-to-noise
522 ratio, thus reducing the statistical reliability of parameter estimation.

523 It is clear that several motion-related factors can potentially impact the accuracy and/or precision of
524 reconstructed images and estimated regional end-point parameters in our approach:

- 525 (i) Potential resolution loss due to insufficient motion sampling and/or off-centre animal
526 locations;
- 527 (ii) Potential increased noise due to periods of unknown motion (blind spots) and/or loss of
528 counts when the animal is outside the FOV.

529 In general, resolution loss is a minor effect (Angelis et al. 2018). The use of high frame-rate
530 tracking (30 Hz) mitigates motion sampling-related error (Angelis et al. 2015, Kyme et al. 2011)
531 and lateral movement of the robotic enclosure allows us to minimise the time the animal is located
532 off-centre transaxially. We used a spatially invariant kernel for resolution modelling which is
533 optimal at the centre (Angelis et al. 2015). A spatially variant kernel (Bickell et al. 2016) may

534 provide further improvement but we have not investigated this. Regarding noise, the inter-voxel
535 variance of a uniform ROI certainly increases as a function of the duration of the tracking gap or
536 loss of counts, however we have also observed that bias remains $<0.5\%$ even when the decrease in
537 counts is $>90\%$ (unpublished data). We are currently seeking to address several of the motion-
538 related factors impacting performance by developing a modified open-field PET system that
539 translates a lightweight PET detector ring in response to gross animal movements rather than the
540 enclosure (Kyme et al. 2017), thus enabling rapid movements without startling the animal and
541 without loss of data.

542 We believe studies of reward-driven learning and plasticity will be an important area of application
543 for the open-field PET technique. To move this field forward, the capacity to measure endogenous
544 neurotransmitter release at the whole-brain level with accurate estimation of the location and timing
545 of activation onset, while simultaneously recording behavioural responses, is essential if we are to
546 gain new insights into the role of specific brain circuits and neurotransmitters in mediating reward
547 prediction and behavioural adaptation. The design of the animal enclosure as an operant
548 conditioning chamber facilitates such studies where, instead of drug administration, the animal
549 learns a contingency between a visual or auditory stimulus and a reward. Other important
550 applications include drug addiction studies and investigations of pathological conditions, such as
551 post-traumatic stress disorder, that impede the ability of an animal to respond appropriately to
552 external stimuli and adapt to a changing environment.

553
554
555
556

557 **Acknowledgements**

558 The authors gratefully acknowledge the following people for their advice and input on various
559 aspects of this work: Richard Banati, Jonathon Arnold, Marie-Claude Grégoire, Arkadiusz Sitek,
560 Marc Normandin and Nathaniel Alpert. This work was supported by the Australian Research
561 Council (project grants DP0988166, DP120103813 and DP160105070) and the Australian Institute
562 for Nuclear Science and Engineering (project grant ALNGRA15022). All work was conducted at
563 the Sydney-ANSTO node of the Australian National Imaging Facility (www.anif.org.au) which is
564 supported by the Commonwealth Government of Australia, the NSW Government, the University
565 of Sydney and the Australian Nuclear Science & Technology Organisation (ANSTO). For part of
566 this work, Andre Kyme was supported by a Cassen Postdoctoral Fellowship, Education and
567 Research Foundation, Society Nuclear Medicine and Molecular Imaging, USA.

568

569 **Declaration of interests:** None

570

571

572 **References**

- 573 Alpert, M. *et al* A novel method for noninvasive detection of neuromodulatory changes in specific
574 neurotransmitter systems. *Neuroimage* **19**(3), 1049-60 (2003).
- 575 Angelis GI, Bickell M, Kyme A, Ryder W, Zhou L, Nuyts J, Meikle S and Fulton R Calculated
576 attenuation correction for awake small animal brain PET studies. *Proc. 2013 IEEE Nucl. Sci.*
577 *Symp. Med. Imaging Conf.* Doi: 10.1109/NSSMIC.2013.6829263 (2013).
- 578 Angelis, G. *et al* Full field spatially-variant image-based resolution modeling reconstruction for the
579 HRRT. *Physica Medica* **31**(2), 137-145 (2015).
- 580 Angelis, G. *et al* Image-based modelling of residual blurring in motion corrected small animal PET
581 imaging using motion dependent point spread functions. *Biomed. Phys. Eng. Express* **4**
582 035032 (2018).
- 583 Angelis, G. I., Kyme, A. Z., Ryder, W. J., Fulton, R. R. & Meikle, S. R. Attenuation correction for
584 freely moving small animal brain PET studies based on a virtual scanner geometry. *Phys.*
585 *Med. Biol.* **59**, 5651–5666 (2014).
- 586 Baba, J. *et al* Molecular imaging of conscious, unrestrained mice with AwakeSPECT. *J Nucl Med.*
587 **54**(6) 969-76 (2013).
- 588 Belle, A. M., Owesson-White, C., Herr, N. R., Carelli, R. M. & Wightman, R. M. Controlled
589 iontophoresis coupled with fast-scan cyclic voltammetry/electrophysiology in awake, freely
590 moving animals. *ACS Chem Neurosci* **4**, 761–771 (2013).
- 591 Bickell, M. *et al* Spatially variant resolution modelling for iterative list-mode PET reconstruction.
592 *IEEE Trans. Med. Imaging* **35**(7), 1707-1718 (2016).
- 593 Chatziioannou, A. F. Molecular imaging of small animals with dedicated PET tomographs. *Eur J*
594 *Nucl Med* **29**, 98–114 (2002).
- 595 Chen, J. L., Andermann, M. L., Keck, T., Xu, N.-L. & Ziv, Y. Imaging Neuronal Populations in
596 Behaving Rodents: Paradigms for Studying Neural Circuits Underlying Behavior in the
597 Mammalian Cortex. *J. Neurosci.* **33**, 17631–17640 (2013).
- 598 Cherry SR (2011) Functional whole-brain imaging in behaving rodents *Nat Methods* **8** (4) 301-3.
- 599 Helmchen, F., Fee, M. S., Tank, D. W., Denk, W. & Hill, M. A miniature head-mounted
600 neurotechnique two-photon microscope: high-resolution brain imaging in freely moving
601 animals. *Neuron* **31**, 903–912 (2001).
- 602 Hillegaart, V., Ahlenius, S. Effects of raclopride on exploratory locomotor activity, treadmill
603 locomotion, conditioned avoidance behaviour and catalepsy in rats: behavioural profile
604 comparisons between raclopride, haloperidol and preclamol. *Pharmacol. Toxicol.* **60**(5) 350-4

- 605 (1987).
- 606 Hume, S. P. *et al* Effect of L-dopa and 6-hydroxydopamine lesioning on [11C]raclopride binding in
607 rat striatum, quantified using PET. *Synapse* **21**, 45–53 (1995).
- 608 Hume, S. P., Gunn, R. N. & Jones, T. Pharmacological constraints associated with positron
609 emission tomographic scanning of small laboratory animals. *Eur. J. Nucl. Med.* **25**, 173–176
610 (1998).
- 611 Ichise, M. *et al* Linearized reference tissue parametric imaging methods: application to [11C]DASB
612 positron emission tomography studies of the serotonin transporter in human brain. *J Cereb*
613 *Blood Flow Metab* **23**, 1096–1112 (2003).
- 614 Kelley, A. E. in *Current Protocols in Neuroscience* (eds. Crawley, J. N. et al) 8.8.1-8.8.13 (John
615 Wiley & Sons, 1998).
- 616 Kyme, A. Z., Zhou, V. W., Meikle, S. R. & Fulton, R. R. Real-time 3D motion tracking for small
617 animal brain PET. *Phys Med Biol* **53**, 2651–2666 (2008).
- 618 Kyme, A. Z., Zhou, V. W., Meikle, S. R., Baldock, C. & Fulton, R. R. Optimised motion tracking
619 for positron emission tomography studies of brain function in awake rats. *PLoS One* **6**,
620 e21727. doi:10.1371/journal.pone.0021727 (2011).
- 621 Kyme, A., Meikle, S., Baldock, C. & Fulton, R. Tracking and characterizing the head motion of
622 unanaesthetized rats in positron emission tomography. *J. R. Soc. Interface* **9**, 3094–3107
623 (2012).
- 624 Kyme, A. *et al* Markerless motion tracking of awake animals in positron emission tomography.
625 *IEEE Trans. Med. Imaging* **33**(11), 2180-90 (2014).
- 626 Kyme, A. *et al* Open-field mouse brain PET: design optimisation and detector characterisation.
627 *Phys. Med. Biol.* **62**, 6207 (2017).
- 628 Lindquist, M. P. & Gotestam, K. G. Open-field behavior after intravenous amphetamine analogues
629 in rats. *Psychopharmacology (Berl)*. **55**, 129–133 (1977).
- 630 Marin, J. M., Pudlo, P., Robert, C. P. & Ryder, R. J. Approximate Bayesian computational
631 methods. *Stat. Comput.* **22**, 1167–1180 (2012).
- 632 Martin, C., Martindale, J., Berwick, J. & Mayhew, J. Investigating neural-hemodynamic coupling
633 and the hemodynamic response function in the awake rat. *Neuroimage* **32**, 33–48 (2006).
- 634 Miranda, A. *et al* Markerless rat head motion tracking using structured light for brain PET imaging
635 of unrestrained awake small animals. *Phys. Med. Biol.* **62**(5), 1744-58 (2017).
- 636 Miranda, A. *et al* Fast and accurate rat head motion tracking with point sources for awake brain
637 PET. *IEEE Trans. Med. Imaging* **36**(7), 1573-82 (2018).
- 638 Mizuma, H., Shukuri, M., Hayashi, T., Watanabe, Y. & Onoe, H. Establishment of in vivo brain
639 imaging method in conscious mice. *J. Nucl. Med.* **51**, 1068–1075 (2010).

- 640 Nakao, Y. *et al* Effects of anesthesia on functional activation of cerebral blood flow and
641 metabolism. *Proc Natl Acad Sci* **98**, 7593–7598 (2001).
- 642 Normandin, M. D., Schiffer, W. K. & Morris, E. D. A linear model for estimation of
643 neurotransmitter response profiles from dynamic PET data. *Neuroimage* **59**, 2689–2699
644 (2012).
- 645 Ohba, H., Harada, N., Nishiyama, S., Kakiuchi, T. and Tsukada, H. Ketamine/xylazine anesthesia
646 alters [11C]MNPA binding to dopamine D2 receptors and response to methamphetamine
647 challenge in monkey brain. *Synapse* **63**, 534–537 (2009).
- 648 Patel, V. D., Lee, D. E., Alexoff, D. L., Dewey, S. L. & Schiffer, W. K. Imaging dopamine release
649 with positron emission tomography (PET) and 11C-raclopride in freely moving animals.
650 *Neuroimage* **41**, 1051–1066 (2008).
- 651 Perkins, G., Sheth, R., Greguric, I. & Pascali, G. Optimisation of [11C]Raclopride production using
652 a Synthra GPextent system. *Curr. Radiopharm.* **7**, 100–106 (2014).
- 653 Rahmim, A. *et al* Accurate event-driven motion compensation in high-resolution PET incorporating
654 scattered and random events. *IEEE Trans. Med. Imaging* **27**, 1018–1033 (2008).
- 655 Schiorring, E. An open field study of stereotyped locomotor activity in amphetamine-treated rats.
656 *Psychopharmacology (Berl)*. **66**, 281–287 (1979).
- 657 Schulz, S. *et al* Simultaneous assessment of rodent behavior and neurochemistry using a miniature
658 positron emission tomograph. *Nat Methods* **8**, 347–352 (2011).
- 659 Tai, Y. C. *et al* Performance evaluation of the microPET focus: a third-generation microPET
660 scanner dedicated to animal imaging. *J Nucl Med* **46**, 455–463 (2005).
- 661 Tantawy, M. *et al* Impact of isoflurane anesthesia on D2 receptor occupancy by [18F]fallypride
662 measured by MicroPET with a modified logan plot. *Synapse* **65**(11), 1173–80 (2011).
- 663 Thanos, P. K. *et al* Mapping brain metabolic connectivity in awake rats with μ PET and optogenetic
664 stimulation. *J. Neurosci.* **33**, 6343–6349 (2013).
- 665 Tsukada, H., Miyasato, K., Kakiuchi, T., Nishiyama, S., Harada, N. and Domino, E.F. Comparative
666 effects of methamphetamine and nicotine on the striatal [11C]raclopride binding in
667 unanesthetized monkeys. *Synapse* **45**, 207–212 (2002).
- 668 Vaska, P. RatCAP: miniaturized head-mounted PET for conscious rodent brain imaging. *IEEE*
669 *Trans Nucl Sci* **51**, 2718–2722 (2004).
- 670 Vyazovskiy, V. V *et al* Local sleep in awake rats. *Nature* **472**, 443–447 (2011).
- 671 Zhou, V. W., Kyme, A. Z., Meikle, S. R. & Fulton, R. R. An event driven motion correction
672 method for neurological PET studies of awake laboratory animals. *Molec Imag Biol* **10**, 315–
673 324 (2008).
- 674 Zhou, V. *et al* A motion adaptive animal chamber for PET imaging of freely moving animals. *IEEE*

675 *Trans Nucl Sci* **60**, 3423–3431 (2013).

676

677

678

679 **Author contributions**

680 SRM and RRF conceived the open-field PET method. AZK, JE, VZ, GH, BB and SRM developed
681 the observation chamber; AZK, RRF and VZ developed the motion tracking methodology; JE, AZK
682 and VZ developed the robot control algorithm; GA, RRF, VZ, WR, AZK, MA and SRM developed
683 the motion correction and image reconstruction methodology; G Pascali and G Perkins produced
684 and optimised the radiotracer; KC and GH performed surgery; GA, GH, AZK and KP trained the
685 animals; GA, AZK, GH, JE, KP and AP performed the PET studies; GA, SRM, GH and AZK
686 performed data analysis; AZK, GA and SRM prepared the manuscript; all authors read and edited
687 the manuscript.

